DOI: 10.1002/adma.200800137

Fabrication of Vertically Aligned Single-Crystalline Boron Nanowire Arrays and Investigation of Their Field-Emission Behavior**

By *Fei Liu, Jifa Tian, Lihong Bao, Tianzhong Yang, Chenming Shen, Xinyu Lai, Ziming Xiao, Weiguo Xie, Saozi Deng, Jun Chen, Juncong She, Nisheng Xu,** and *Hongjun Gao**

Elemental boron arouses great interest from both scientific and technological areas of research because it has unique chemical and physical properties and its theoretical tubular structures may have higher electrical conductivity than carbon nanotubes.[1–7] High conductivity and chemical stability of boron or boride nanostructures have made it an attractive candidate for future applications in ideal cold-cathode materials, high-temperature semiconductor devices, or field-effect transistors.[8–14] In particular, for the application of field emission (FE), it is especially useful to synthesize large, vertical arrays of boron nanowires (BNWs) with the desired surface work function and FE behavior. So far, to our knowledge, while both amorphous[15–20] and crystalline boron nanowires[21,22] have been fabricated by magnetron sputtering, laser ablation, or chemical vapor methods, vertical arrays of single-crystal boron nanowires over a large area have not been synthesized in a one-step process. In addition, little attention[23–25] has been paid to the measurements of the physical properties of an individual boron nanowire.

In this Communication, we report the successful synthesis of high-density, vertically aligned single-crystal boron nanowire arrays with a nanowire diameter of approximately 20–40 nm by a thermal carbon-reduction method. Moreover, we have measured the FE behavior and surface work function of a single boron nanowire, which is critical to evaluate the possibility of using boron nanowires as field-emission materials. For the purpose of better understanding the field-emission mechanism of a boron nanowire, the field-emission properties of a BNW film are also measured to compare with those of an individual nanowire.

Figure 1 shows large-scale boron nanowire arrays on a Si(001) substrate after approximately 2–4 h of growth. As shown in Figure 1A, the high-density arrays are aligned vertically on the silicon substrate. Figure 1B is the high-resolution scanning electron microscopy (SEM) image of the aligned BNWs, in which one can see that the length of the BNW is about 5 μm and the morphology of the nanowires is uniform. The aspect ratio of each boron nanowire is about 200, which is high enough for a field-emission application. The side and top views of the boron nanowire are shown in Figure 1C and D, respectively, which reveals the detailed morphology of the BNWs. The boron nanowires have a diameter of about 20–40 nm and no catalyst is found at their tip. The catalysts, however, were found to lie on the substrate arbitrarily when we peeled off some nanowire film from the substrate, as shown in Figure 1C. Thus, we believe that the growth is through a vapor–liquid–solid (VLS) mechanism and the binding force between the Fe_3O_4 catalyst and the silicon substrate is strong. This strong binding leads to good conductivity between the boron nanowires and the substrate, which may contribute to their good field-emission properties. The alignment of BNWs can be attributed to steric overcrowding.[26,27]

To determine the detailed crystalline structure, transmission electron microscopy (TEM) and high-resolution TEM (HRTEM) were employed to investigate the sample. A typical TEM image of the boron nanowires is shown in Figure 2A. The diameter of all the nanowires is rather uniform. Figure 2B shows the corresponding HRTEM image of the boron nanowire indicated by the white arrow in Figure 2A. By analyzing the HRTEM image, we found that the boron nanowire has clear lattice fringes and the *d* spacing between the adjacent (002) planes is 5.06 Å. In addition, an amorphous sheath of about 1.5 Å appears in this HRTEM image, which most likely originates from boron oxide. The boron nanowire has a single-crystalline structure as indicated by the sharp diffraction spots in the inset (acquired from the same nanowire). The growth of these boron nanowires is along

[*] Prof. N. S. Xu, Dr. F. Liu, X. Y. Lai, Z. M. Xiao, W. G. Xie, S. Z. Deng J. Chen, J. C. She
State Key Laboratory of Optoelectronic Materials and Technologies
Guangdong Province Key Laboratory of Display Material and Technology, and
School of Physics and Engineering, Sun Yat-sen University
Guangzhou 510275 (P.R. China)
E-mail: stsxns@mail.sysu.edu.cn
Prof. H.-J. Gao, Dr. J. F. Tian, L. H. Bao, T. Z. Yang, C. M. Shen
Beijing National Laboratory for Condensed Matter Physics
Institute of Physics, Chinese Academy of Sciences
Beijing 100080 (P.R. China)
E-mail: hjgao@aphy.iphy.ac.cn

[**] This work is supported by the National Basic Research Program of China (973 Program, Grant No. 2007CB935500, 863 Program, Grant No. 2007AA03Z305), the National Joint Science Fund with Guangdong Province (Grant No. U0634002, U0734003), the Doctoral Foundation of Education Ministry of China (Grant No. 20070558063), the Science and Technology Department of Guangdong Province, the Education Department of Guangdong Province, and the Science and Technology Department of Guangzhou City.

ADVANCED MATERIALS

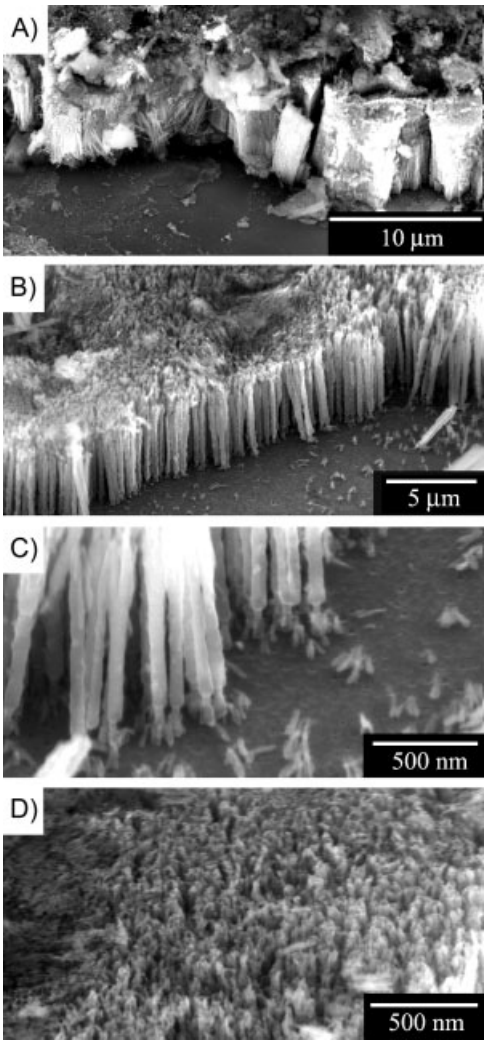

Figure 1. Scanning electron microscopy (SEM) images of vertically aligned boron nanowire arrays. A) Low-magnification image of large-area arrays. B) High-resolution image of boron nanowires. C,D) Top and side view, respectively, of the boron nanowires.

the [001] direction, which is in agreement with the data of the Joint Committee for Powder Diffraction Standards (JCPDS) card No. 73-0511. Combining the HRTEM result with the selected-area electron diffraction pattern, we conclude that the boron nanowires are perfect single crystals with an α-tetragonal structure.

Because boron and boron oxide powders are used as the source materials, we use the elemental maps of boron and oxygen to identify the elemental distribution in an individual boron nanowire. Figure 2C and D offers the elemental distribution images of boron and oxygen, respectively, in the same nanowire. It is noted that the bright region corresponds to the distribution of the measured element. The insets exhibit the elemental profiles of boron and oxygen across the nanowire, which clearly shows that boron is uniformly distributed through the whole nanowire, while oxygen only exists at the sheath of the nanowire. The formation of boron oxide is likely caused by the exposition of the as-grown boron nanowire to the air after the reaction. The possible explanation of oxidation is given as follows. Firstly, boron nanowires have a large surface area, which suggests they possess many active surface states and, thus, their oxidation in air is easier than bulk boron materials in air. Secondly, the physical property measurements were carried out about two months after the BNWs were fabricated; thus, slow oxidation might have occurred in the interim period. However, the oxidation will be terminated after about 2–3 Å of oxide layer are formed on the BNWs because the layer is too compact to keep oxidation of the BNW going. From the HRTEM results, we conclude that the oxidation speed is approximately 1–1.5 Å/month. Further quantitative elemental analysis was performed on the boron nanowire by using EELS (electron energy loss spectroscopy). Gatan EELS analysis software demonstrates that the total content of boron in the boron nanowire is over 95% and traces of oxygen can only be found in the highly magnified EELS spectrum. Only a small amount of elemental carbon (less than 4%) can be detected with EELS, which may come from the circumstancial C adsorption or the carbon film in the copper grid used in HRTEM. So the samples are single-crystal boron nanowires with an oxide sheath, which is consistent with the previous HRTEM results in Figure 2B.

The as-prepared boron nanowires have potential for applications in the field-emission area because they are perfect single crystals in a vertical array and have high aspect ratios. Among the field-emission parameters, the work function value is very important. Although bulk boron materials have a mean work function of 4.6 eV and bandgap of 1.56 eV,[1,28] the surface work function of an individual boron nanowire is unknown. Because Kelvin probe force microscopy (KPFM)[29,30] technology is a powerful technique for measuring the work function of a material at the nanoscale, we applied this technique in the Omicron VT-AFM system to characterize the work function of an individual boron nanowire. Figure 3 provides the topography and contact potential difference (CPD) images of a single BNW. As seen in Figure 3A, a typical boron nanowire has a mean radius of about 30 nm. Figure 3B shows a high-resolution image with clear contrast. The bright region, which has a higher conductivity, possesses a high contact potential and, therefore, a low work function. Using the work function of a standard highly oriented pyrolytic graphite (HOPG) as reference, we obtain the work function value of the atomic force microscopy (AFM) probe to be 4.0 eV. From the CPD image, the mean value of V_{CPD} between the probe and the nanowire is deduced to be about −0.4 V. So the surface work function of a single boron nanowire is about 4.4 eV, which is slightly lower than that of bulk boron. The work function is found to be uniform through the nanowire with the exception of the end of the nanowire, which shows a lower work function because of the presence of the Fe_3O_4 catalyst that is known to have a work function of 3.7 eV. Other regions of magnetite catalyst nanoparticles also exhibit a similar lower work function than boron nanowires in the KPFM images, which

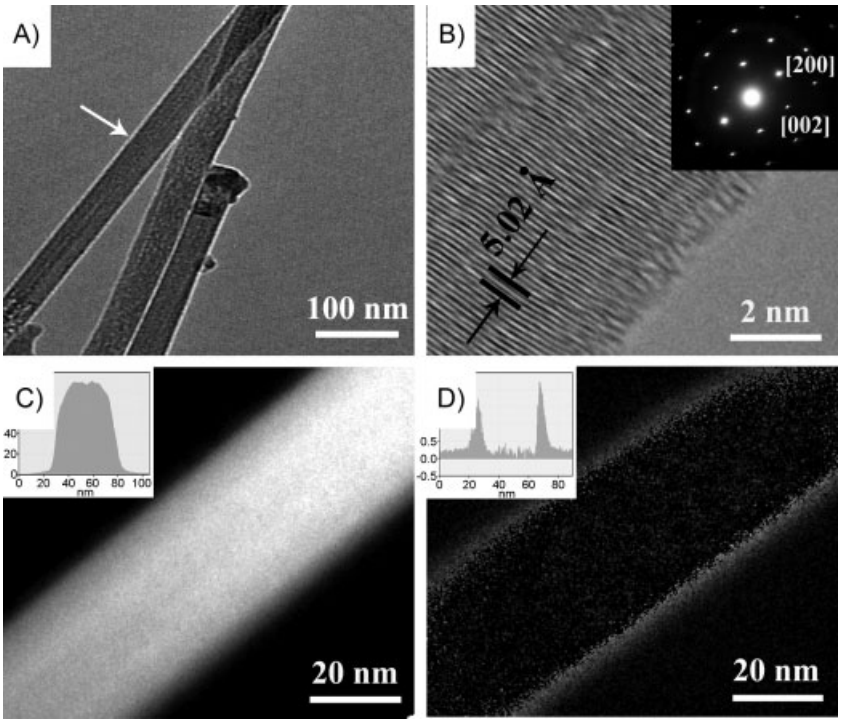

Figure 2. A) A typical TEM image of the BNWs. B) A HRTEM image of the BNW (indicated by the white arrow in (A)). The inset is the corresponding selected-area electron diffraction pattern. C,D) The elemental maps of boron and oxygen, respectively, of the same nanowire. The insets correspond to the B and O elemental profiles across this nanowire.

agrees with the AFM image in Figure 3A. If the oxide sheath of the BNW is taken into account, the actual work function value of a single-crystal boron nanowire should be slightly lower than 4.4 eV. According to the Fowler–Nordheim (FN) theory, the nanowire will have better field-emission performance if its work function is lower. Although the surface work function value of a pure boron nanowire may not be low enough to serve as an ideal cold cathode material, doping some elements (for example C, N, and Fe) into the nanowire should efficiently decrease the surface work function value; such efforts are under way.

To further evaluate the feasibility of applying BNWs in the vacuum microelectronic and nanoelectronic fields, we have measured the field-emission properties of an individual boron nanowire in a modified high-vacuum SEM system.[31] To our knowledge, this is the first report on the FE properties of a single boron nanowire. Figure 4A and 4B shows the SEM images of the tungsten probe and a single boron nanowire, which were used in the measurement. The detailed measurement procedure is described as follows: First, the tungsten probe is moved to contact an individual BNW, and the resistance between them is recorded by a pico-amperemeter (Keithley 6487). The detected voltage on the probe is −5 V. This step is adopted to ensure the alignment as well as the ohmic contact between the probe and the boron nanowire during the measurements. Second, the W probe is retracted to a distance of 1.507 μm from the individual boron nanowire by a stepped motor. As soon as the probe leaves the individual nanowire, the reading data of the pico-amperemeter returns to zero. Last, the field-emission current data are auto-recorded by the Keithley 6487 RS232 instrument software as a function of the applied voltage up to 200 V in steps of about 0.5–1 V. We measured many individual BNWs, and they display three representative curves of current versus electric field (*I–E*), as shown in Figure 5, where A, B, and C refer to three different boron nanowires. When an electric field of approximately 59–74 V μm^{-1} is applied, a stable FE current of 1 μA is reached. Considering the average curvature radius of an individual nanowire is 15 nm, we calculate the maximum emission current density to be about 2×10^5–4×10^5 A cm^{-2}. Such a high current density indicates that a BNW may be an excellent candidate for a high-brightness point electron source. Further investigation shows that a FE current of 0.1 nA for an individual boron nanowire is obtained at an average electric field of 10–14 V μm^{-1}. The current density is around 20–28 A cm^{-2}, corresponding to the emission current of 0.1 nA.

These three boron nanowires exhibit slight differences in their FE behavior, as shown in Figure 5A, in which nanowire A has the best and nanowire C has the worst field-emission behavior, but we can not find any distinguishable difference in their morphologies from their corresponding SEM images. For further understanding of the FE mechanism of an individual BNW, we measured the conductance of these three nanowires at the same time (Fig. 5B). Through detailed measurements, we find that these three nanowires (A–C) possess different electrical conductivity of nanowire A is the highest (ca. $8\times10^{-3}\,\Omega^{-1}\,cm^{-1}$) and that of nanowire C is the lowest (ca. $3.2\times10^{-3}\,\Omega^{-1}\,cm^{-1}$), which possibly induces their different FE properties. It is suggested that an individual boron nanowire will have a better field-emission performance if it has a lower resistance. There are other factors that influence the FE properties of individual BNWs, and they are illustrated as follows. Firstly, the boron nanowires have different aspect ratios, which may lead to their different conductance values. Secondly, the thickness of the surface oxide layer on different BNWs is not the same. Thirdly, there are some different crystalline defects existing in boron nanowires as revealed by magnified HRTEM investigations although they appear to be single crystals in TEM images. A more detailed explanation of the influence of these factors will be discussed in our forthcoming paper.[32] All of the measured BNWs have similar FE characteristics without breaking down, up to 4 μA, during our FE measurements, which suggests they can operate at high temperature. These results are comparable to the best results

ADVANCED MATERIALS

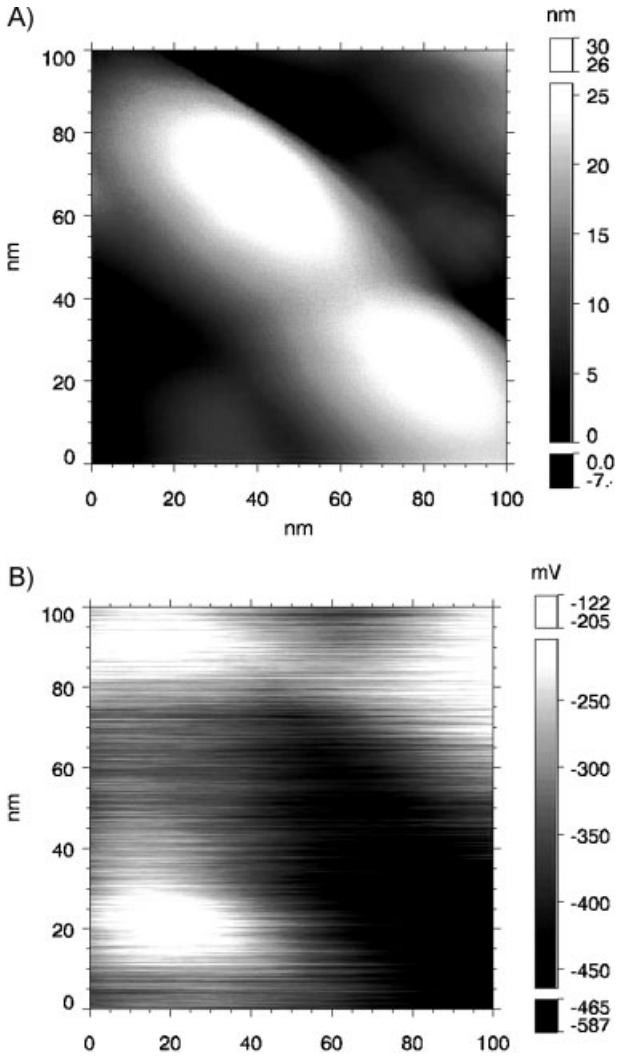

Figure 3. KPFM (Kelvin probe force microscopy) and simultaneous measurement of topography on a single boron nanowire. A) Atomic force microscopy (AFM) image of a single boron nanowire. B) The corresponding CPD (contact potential difference) image of the same boron nanowire.

from other nanowires that are considered to have excellent FE properties.[31,33–35]

The Fowler–Nordheim (FN) equation is used to describe the metal–vacuum field-emission model, in which good linearity of the FN plots means the cathode material agrees with this model and is close to the behavior of metal. The typical FN plot, $\ln(I/E^2)$ versus $1/E$, is shown in Figure 5C. According to the FN theory, the relationship between current density (J) and applied electric field (E) can be described as follows:[36]

$$J = A\left(\frac{\beta^2 E^2}{\phi}\right)\exp\left(\frac{-B\phi^{\frac{3}{2}}}{\beta E}\right) \quad (1)$$

where $A = 1.57\times10^{-10}\,\mathrm{A\,V^{-2}\,eV}$, $B = 6.83\times10^{9}\,\mathrm{V m^{-1}\,eV^{-3/2}}$, and ϕ is the work function of a single boron nanowire, which

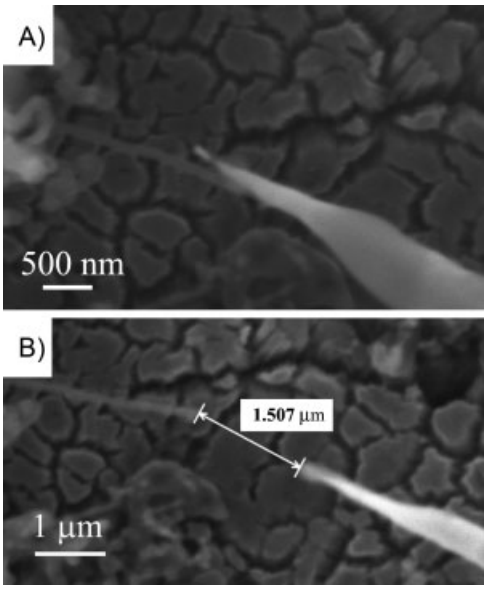

Figure 4. SEM images of the single boron nanowire during FE measurements. SEM images of the W probe and the single nanowire A) before and B) during the measurement.

is 4.4 eV, as obtained in our KPFM measurement. The enhancement factor β is calculated to be about 2000–2500 at low electric fields, and 50–800 at high electric fields. The wide range of β implies the versatility for various FE applications. As for the nonlinear behavior of the FN plot and the better field emission at high current, we propose two possible mechanisms: 1) Field electron emission is enhanced by the emission of thermal electrons at high temperature caused by the high current; 2) The conductivity of the BNW is enhanced because of the thermal vaporization of boron oxide from its surface at high temperature, which improves the field electron emission properties at high current. The detailed physical mechanism is still under investigation.

We have also measured the FE behavior of a large-area BNW film to compare with that of an individual boron nanowire. Figure 6 shows the field-emission curve of current density versus electric field (J–E) from a large-scale boron nanowire film. The turn-on electric field (E_{on}) and the threshold electric field (E_{thres}) of the BNW film are $5.1\,\mathrm{V\,\mu m^{-1}}$ ($J=10\,\mu\mathrm{A\,cm^{-2}}$) and $11.5\,\mathrm{V\,\mu m^{-1}}$ ($J=1\,\mathrm{mA\,cm^{-2}}$), respectively. When increasing the electric field to $17.8\,\mathrm{V\,\mu m^{-1}}$, a higher current density of $8.1\,\mathrm{mA\,cm^{-2}}$ can be obtained with no saturation tendency in this experiment. The E_{thres} value of the BNW film is higher than that of carbon nanotubes ($1.6\,\mathrm{V\,\mu m^{-1}}$)[37] and tungsten oxide nanowires ($6.2\,\mathrm{V\,\mu m^{-1}}$)[38] but is close to that of aligned In_2O_3 nanowires ($10.8\,\mathrm{V\,\mu m^{-1}}$).[39] As a very high density of one-dimensional nanowires is often harmful to field electron emission because of the screen effects,[40,41] we have attempted the following experiments to control the density of the vertically aligned boron nanowires at the optimized theoretical values[42,43] to

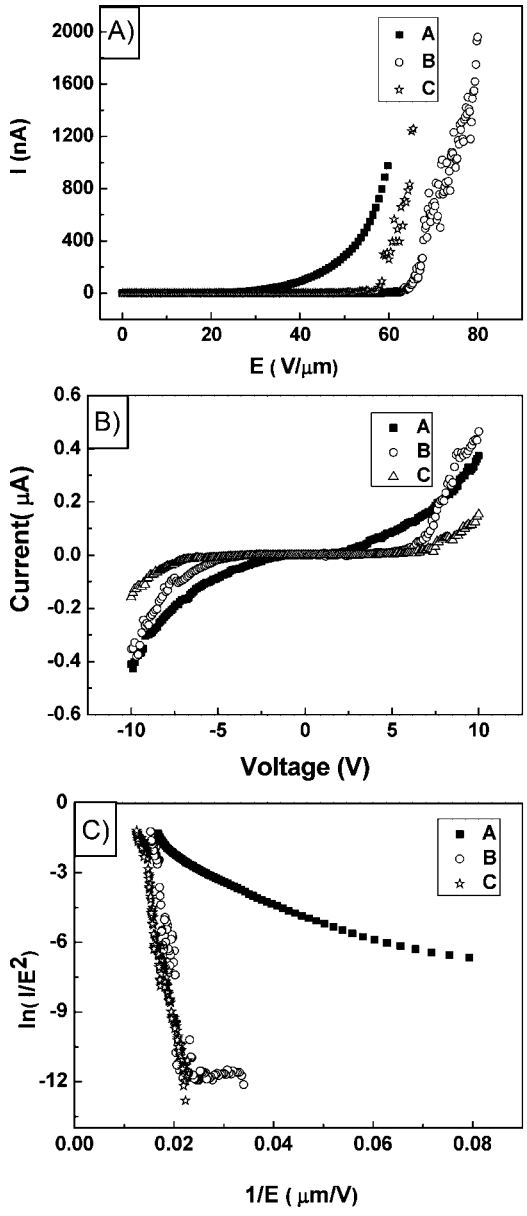

Figure 5. A) The current–electric field (*I*–*E*) curves of individual boron nanowires: A, B, C refer to the three different boron nanowires. B) The corresponding current–voltage (*I*–*V*) curves of these three individual boron nanowires (A–C) in FE measurements. C) The corresponding FN plots of these three BNWs.

decrease the E_{on} and E_{thres} values. The inset of Figure 6 is the FN plot of the film of aligned BNWs. The FN plots is almost linear, agreeing well with the FN theory. The field-emission behavior of the aligned BNW film at high current density, however, is different from that of an individual boron nanowire. A possible interpretation is that for the film, the proportion of the thermal electron current in the measured field-emission current at high current density is too small to show its contribution to the tendency of the FN plot. The real FE properties and the detailed FE mechanism of boron

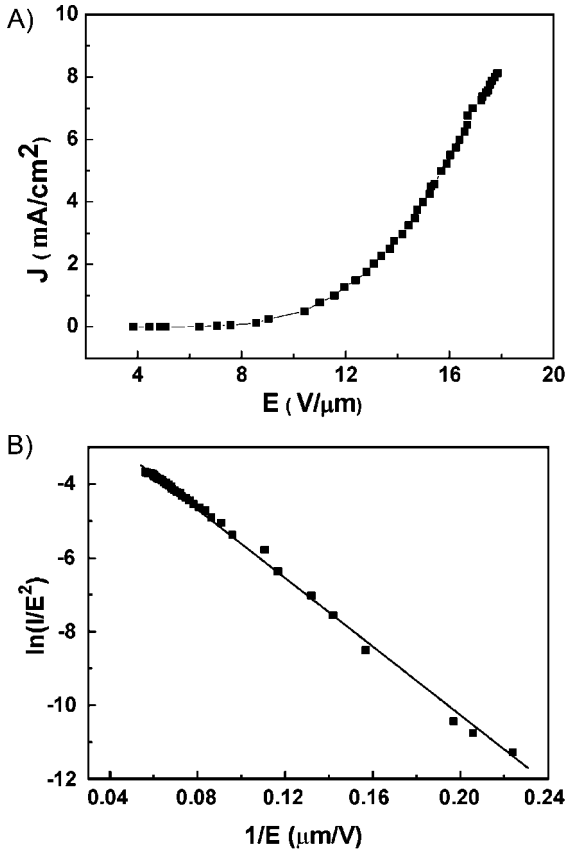

Figure 6. A) The *J*–*E* field-emission curve of a large-area film of vertically aligned boron nanowires. B) FN plot of this sample.

nanowires are difficult to understand because they are concealed by the field-emission behavior of the nanostructured thin film, and further investigation is still needed.

Finally, we have measured the emission stability of an individual boron nanowire at high working current, which is critical for a cold-cathode material. Figure 7 shows the

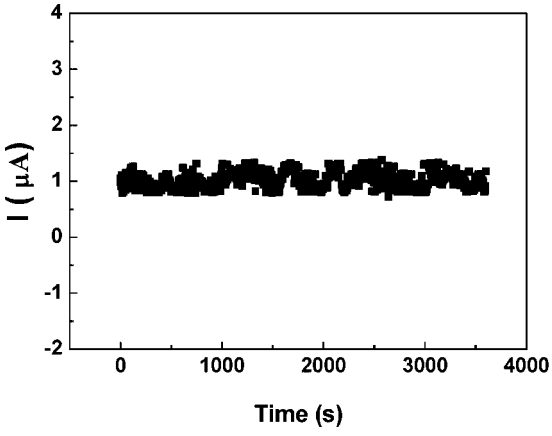

Figure 7. The representative emission stability curve of the individual boron nanowire at high current.

ADVANCED MATERIALS

representative emission stability curve of in individual BNW at high current. The DC voltage is fixed at 200 V and the whole measurement lasted for 1 h. It is evident that the boron nanowire exhibits a stable field emission at a high current of 1.05 μA with a fluctuation of less than 22% through the continuous high-current operation. This 22% instability at high current is acceptable for the following reasons: 1) Part of the fluctuation comes from vacuum pump vibrations, which give rise to a slight change of the distance between the probe and the sample during the FE measurements; 2) At more commonly used lower working currents, the stability should be considerably improved, as reported in our recent work.[23,32] Our recent results show that an individual boron nanowire has a higher conductivity of 1.4×10^{-3}–$8.0\times10^{-3}\,\Omega^{-1}\cdot cm^{-1}$ than that of bulk boron materials (10^{-5}–$10^{-6}\,\Omega^{-1}\cdot cm^{-1}$).[1,2,5] Good conductivity means low turn-on fields and high endurable ability at high current, which are favorable to its practical application in FE displays. The effect of the morphology, crystallinity, and contact conductance of the individual boron nanowires on their FE properties is under investigation because these measurements could provide more decisive interpretations on the field-emission mechanism.

In summary, arrays of vertically aligned single-crystal boron nanowires, which have a diameter of about 30 nm, have been successfully fabricated over a large area by a thermal carbon-reduction method. The BNWs are perfect single crystals with a tetragonal structure and have a growth direction along [001]. The work function and field-emission behavior from an individual boron nanowire are measured for the first time and compared with those from films of high-density aligned boron nanowires. FE properties and KPFM measurements on a single boron nanowire show that its emission current density should reach 2×10^5–4×10^5 A cm^{-2} at the electric field of 5–74 V μm^{-1} and it has a work function of about 4.4 eV. In addition, the as-prepared BNWs are proved to have a high enhancement factor, good emission stability, and can endure high current. These experimental results suggest that a boron nanowire can be an excellent FE material candidate and has a promising future in field-emission applications.

Experimental

Large-scale, aligned BNW arrays in these experiments were grown by a thermal carbon-reduction method in a single-stage furnace developed in our group [26,27]. The only difference in our description of the method is that, in the present work, site A and B refer to upstream of the mixed gases' flow and the center of the furnace, respectively. Fe_3O_4 nanoparticles with a diameter of less than 10 nm were synthesized by a high-temperature, solution-phase reaction method [44,45].

B_2O_3 powder (99.99%), B powder (99.99%), and graphite powder (99.99%) were ground together in a mass ratio of 2:4:1 and loaded onto an alumina boat. An Fe_3O_4-coated Si(001) wafer was placed above the vessel as the substrate and remained at site A out of the reaction region before the boron nanowire arrays grew. The temperature, gas flow rate, and evaporation rate of region B could be controlled. When the temperature of the reaction region (Site B) reached 400 °C, the vessel was transferred from site A to site B rapidly and kept there for 20–30 min to eliminate the remaining oleic acid and oleylamine in the first procedure. The flow rate of Ar gas was maintained at 300 sccm throughout this procedure. In the second procedure, when the temperature of region B was increased to 1000–1100 °C at a rate of 20 °C min^{-1}, the growth of the boron nanowire arrays started. The reaction lasted for about 2–4 h in this procedure under a constant flow of argon (ca. 25–30 sccm). The Ar gas in the quartz reaction tube was kept at atmospheric pressure. After the furnace was cooled to room temperature, a dark-brown or black thin film was found on the surface of the substrate.

A field-emission scanning electron microscope (XL-SFEG, FEI Corp.) was used to observe the morphologies of the boron nanowires. Transmission electron microscopy (Tecnai-20, FEI Corp.) and high-resolution transmission electron microscopy (Tecnai F20, FEI Corp.) were used to obtain low-resolution and high-resolution images of BNWs, respectively. FE properties and work functions of single BNWs were performed on the modified SEM system (JEOL-6380)[28] and Omicron VT-AFM system equipped with Kelvin probe force microscopy (KPFM) capability, respectively.

Received: January 15, 2008
Published online: May 15, 2008

[1] *Boron and Refractory Borides*, (Ed: V. I. Matkovich,), Springer, New York **1977**.
[2] *Progress in Boron Chemistry*, (Ed: R. J. Brotherton,), Pergamon, Oxford **1970**.
[3] *Boron, Metallo-Boron Compounds and Boranes*, (Ed: R. M. Adams,), Interscience, New York **1964**.
[4] D. Emin, *Phys. Today* **1987**, *20*, 55.
[5] *Boron Synthesis, Structure, and Properties*, (Ed: J. A. Kohn,), Plenum Press, New York **1973**.
[6] I. Boustani, A. Quandt, E. Hernandez, A. Rubio, *J. Chem. Phys.* **1999**, *110*, 3176.
[7] A. Gindulyte, W. N. Lipscomb, L. Massa, *Inorg. Chem.* **1999**, *37*, 6544.
[8] R. Tenne, A. K. Zetti, *Top. Appl. Phys.* **2001**, *80*, 81.
[9] R. Tenne, *Prog. Inorg. Chem.* **2001**, *50*, 269.
[10] G. R. Patzke, F. Krumeich, R. Nesper, *Angew. Chem. Int. Ed.* **2002**, *41*, 2446.
[11] C. R. Martin, *Science* **1994**, *266*, 1961.
[12] P. M. Ajayan, O. Stephan, Ph. Redlich, C. Colliex, *Nature* **1995**, *375*, 564.
[13] S. M. Yang, I. Sokolov, N. Coombs, C. T. Kresge, G. A. Ozin, *Adv. Mater.* **1999**, *11*, 1427.
[14] U. Kondo, K. Takanayagi, *Science* **2000**, *289*, 606.
[15] Y. Y. Wu, B. Messer, P. D. Yang, *Adv. Mater.* **2001**, *13*, 1487.
[16] L. M. Cao, Z. Zhang, L. L. Sun, C. X. Gao, M. He, Y. Q. Wang, Y. C. Li, X. Y. Zhang, G. Li, J. Zhang, W. K. Wang, *Adv. Mater.* **2001**, *13*, 1701.
[17] L. M. Cao, K. Hahn, Y. Q. Wang, C. Scheu, Z. Zhang, C. X. Gao, Y. C. Li, X. Y. Zhang, L. L. Sun, W. K. Wang, M. Rühle, *Adv. Mater.* **2002**, *14*, 1294.
[18] S. H. Yun, J. Z. Wu, A. Dibos, X. Zou, U. O. Karlsson, *Nano Lett.* **2006**, *6*, 385.
[19] S. H. Yun, J. Z. Wu, A. Dibos, X. Gao, U. O. Karlsson, *Appl. Phys. Lett.* **2005**, *87*(113), 109.
[20] X. M. Meng, J. Q. Hu, Y. Jiang, C. S. Lee, S. T. Lee, *Chem. Phys. Lett.* **2003**, *370*, 825.
[21] Q. Yang, J. Sha, J. Xu, Y. J. Ji, X. Y. Ma, J. J. Niu, H. Q. Hua, D. R. Yang, *Chem. Phys. Lett.* **2003**, *379*, 87.
[22] Y. Zhang, H. Ago, M. Yumura, T. Komatsu, S. Ohshima, K. Uchida, S. Iijima, *Chem.Commun.* **2002**, 2806.
[23] X. J. Wang, J. F. Tian, T. Z. Yang, L. H. Bao, C. Hui, F. Liu, C. M. Shen, N. S. Xu, H.-J. Gao, *Adv. Mater.* **2007**, *19*, 4480.

[24] D. W. Wang, J. G. Lu, C. J. Otten, W. E. Buhro, *Appl. Phys. Lett.* **2003**, *83*, 5280.
[25] K. Kirihara, Z. Wang, K. Kawaguchi, Y. Shimizu, T. Sasaki, N. Koshizaki, K. Soga, K. Kimura, *Appl. Phys. Lett.* **2005**, *86*(212), 101.
[26] F. Liu, P. J. Cao, H. R. Zhang, C. M. Shen, Z. Wang, J. Q. Li, H. J. Gao, *J. Cryst. Growth* **2005**, *274*, 126.
[27] P. J. Cao, Y. S. Gu, H. W. Liu, F. Shen, Y. G. Wang, Q. F. Zhang, J. L. Wu, H. J. Gao, *J. Mater. Res.* **2003**, *18*, 1686.
[28] *Landolt–Bornstein Numerical Data and Functional Relationships in Science and Technology*, New Series (Ed: K. H. Hellwege,), Springer, Berlin **1983**.
[29] Ch. Sommerhalter, Th. W. Matthers, Th. Glatzel, A. Jäger-Waldau, M. Ch. Lux-Steiner, *Appl. Phys. Lett.* **1999**, *75*, 286.
[30] J. M. R. Weaver, D. W. Abraham, *J. Vac. Sci. Technol. B* **1991**, *9*, 1559.
[31] J. C. She, S. An, S. Z. Deng, J. Chen, Z. M. Xiao, J. Zhou, N. S. Xu, *Appl. Phys. Lett.* **2007**, *90*(073), 103.
[32] F. Liu, L. H. Bao, J. F. Tian, C. M. Shen, S. Z. Deng, J. Chen, H. J. Gao, N. S. Xv, in preparation.
[33] H. Zhang, J. Tang, Q. Zhang, G. Zhao, G. Yang, J. Zhang, O. Zhou, L.-C. Qin, *Adv. Mater.* **2006**, *18*, 87.
[34] N. S. Ramgir, I. S. Mulla, K. Vijayamohanan, D. J. Late, A. B. Bhise, M. A. More, D. S. Joag, *Appl. Phys. Lett.* **2006**, *88*(042), 107.
[35] Y. Yu, C. H. Jin, R. H. Wang, Q. Chen, L.-M. Peng, *J. Phys. Chem. B* **2005**, *109*(18), 772.
[36] R. H. Fowler, L. W. Nordheim, *Proc. R. Soc. London, Ser. A* **1928**, *119*, 173.
[37] M. Rao, D. Jacques, R. C. Haddon, W. Zhu, C. Bower, S. Jin, *Appl. Phys. Lett.* **2000**, *76*, 3813.
[38] Y. B. Li, Y. Bando, D. Golberg, *Adv. Mater.* **2003**, *15*, 1294.
[39] S. Q. Li, Y. X. Liang, T. H. Wang, *Appl. Phys. Lett.* **2006**, *88*(053), 107–1.
[40] J.-M. Bonard, K. A. Dean, B. F. Coll, C. Klinke, *Phys. Rev. Lett.* **2002**, *89*(197), 602.
[41] L. Nilsson, O. Groening, C. Emmenegger, O. Kuettel, E. Schaller, L. Schlapbach, H. Kind, J.-M. Bonard, K. Kern, *Appl. Phys. Lett.* **2000**, *76*, 2071.
[42] J.-M. Bonard, N. Weiss, H. Kind, T. Stöckli, L. Forró, K. Kern, A. Châtelain, *Adv. Mater.* **2001**, *13*, 184.
[43] L. Nilsson, O. Groening, P. Groening, O. Kuettel, L. Schlapbach, *J. Appl. Phys.* **2001**, *90*, 768.
[44] H. T. Yang, C. M. Shen, Y. K. Su, T. Z. Yang, H. J. Gao, Y. G. Wang, *Appl. Phys. Lett.* **2003**, *82*, 4729.
[45] S. T. He, J. N. Yao, P. Jiang, Dongxia. Shi, H. Zhang, S. Xie, S. Pang, H. J. Gao, *Langmuir* **2001**, *17*, 1571.

